

Liquid-Phase Growth of Small Crystals for Seeding α -SiAlON Ceramics

M. Zenotchkine, R. Shuba, and I-Wei Chen*

Department of Materials Science and Engineering, University of Pennsylvania, Philadelphia, Pennsylvania 19104-6272

Single-phase small crystals of Li-, Mg-, Ca-, Y-, Nd-, and Yb- α -SiAlONs have been obtained by liquid-phase sintering for various compositions and processing conditions. These crystals are suitable for seeding grain growth in α -SiAlON ceramics. The influence of chemical and processing parameters (starting composition and powders, green density, liquid content, heating schedule, nitrogen pressure, and temperature) on the size and morphology of seed crystals has been investigated. The results are compared with those for β -Si₃N₄ crystal formation, and the differences are discussed in terms of nucleation and growth kinetics during liquid-phase sintering.

I. Introduction

SEEDING is a well-known method for microstructure control that can lead to enhanced properties. For silicon nitride ceramics, seed crystals provide preferential sites for heterogeneous crystallization of the final phase, allowing the control of grain size and grain aspect ratio that are essential for superior fracture toughness. Seed crystals are sometimes available in the native starting powder;¹ for example, both α and β phases are present in most commercial Si₃N₄ powders. Nevertheless, artificial seeds that are more stable than the native ones, because of either a size advantage or a composition advantage, are usually more potent in directing heterogeneous crystallization and microstructure development. Artificial seeding of β -Si₃N₄-based ceramics has been extensively pursued by several groups,^{2–7} resulting in ceramics with improved microstructure and fracture toughness ($K_{IC} = 9–12 \text{ MPa}\cdot\text{m}^{1/2}$).^{4–6} Artificial seeding has also been reported for *in situ* toughened α -SiAlON in several systems.^{8–11} Tough α -SiAlON ceramics with coarse elongated microstructures and high fracture toughness ($9–11 \text{ MPa}\cdot\text{m}^{1/2}$) have been obtained using such a method.¹¹

Seed crystals are typically obtained by a liquid growth process. Preparation of α -SiAlON seed crystals is complicated by the consideration that the parent α -Si₃N₄ phase is thermodynamically unstable under typical liquid growth conditions. It can be stabilized only by forming a solid solution with a formula $M_{m/z}\text{-Si}_{12-m-n}\text{Al}_{m+n}\text{O}_n\text{N}_{16-n}$. (M stands for an interstitial metal ion of valence z .) Nevertheless, with appropriate liquid compositions, it should be possible to vary the size and morphology of liquid-grown α -SiAlON seed crystals by adjusting heat-treatment schedule, nitrogen pressure, the amount of liquid, and the characteristics of starting Si₃N₄ powder. The present work seeks to identify the key factors in the synthesis of α -SiAlON seeds to aid future research and development of α -SiAlON. A preliminary account of this work was already reported elsewhere.¹⁰

II. Background: Phase Equilibrium and Composition

Seed crystals must be stable during the crystal growth process and compatible with the final α -SiAlON ceramics. The latter requirement can be simply met by using seeds that have the same composition as the ceramics. The main issue is to identify liquid compositions that are compatible with α -SiAlON during crystal growth. Phase relations between α -SiAlON and oxynitride liquid phases have been reported in several studies. One class of liquid that is compatible with α -SiAlON has the general composition of $M_2(\text{Si,Al})_3(\text{O,N})_7$ or $M_2\text{O}_z(\text{Si,Al})_3(\text{O,N})_4$. The liquid crystallizes to compounds such as gehlenite ($2\text{CaO}\cdot\text{Al}_2\text{O}_3\cdot\text{SiO}_2$),¹² melilite ($\text{R}_2\text{O}_3\cdot\text{Si}_3\text{N}_4$),¹³ where R is Y or a rare-earth element, or $2\text{CaO}\cdot\text{Si}_3\text{N}_4$, as summarized by the subsolidus phase diagram in Fig. 1(a). Note too that the liquid region usually extends over a broader range at higher temperatures, as shown in Fig. 1(b). Huang *et al.*¹⁴ also reported ternary phase diagrams of $\text{Li}_2\text{O}\text{-Si}_3\text{N}_4\text{-AlN}$ and $\text{MgO}\text{-Si}_3\text{N}_4\text{-AlN}$ systems with similar features. In addition, Jack¹⁵ reported the coexistence between Li- α -SiAlON and Li-eucryptite (LiAlSiO_4) in the $\text{Si}_3\text{N}_4\text{-Li}_2\text{O}\text{-Al}_2\text{O}_3$ system. These studies have provided initial guidelines for formulating liquid compositions for α -SiAlON crystal growth. By adjusting metal oxide content, the chemical composition of crystals can be further tuned to coincide with the desired α -SiAlON composition.

The amount and the viscosity of liquid, in addition to the reaction temperature, are likely to be among the most important factors that influence the kinetics of crystal growth. In the (Si,Al)(O,N) system, viscosity can be adjusted by Al₂O₃ or SiO₂ content, or by temperature. On the other hand, it is well known (e.g., see Ref. 16) that the stability of α -SiAlON depends on the type of modifying cations, but generally increases with temperature. Therefore, seed crystals of the more stable type, e.g., Li-, Ca-, Y-, and Yb- α -SiAlON, can be grown at either low (e.g., 1650°–1700°C) temperature or high temperature, whereas seed crystals of the less stable Nd- and Mg- α -SiAlON type must demand a higher growth temperature (e.g., 1850°–1900°C). In the compositional space, a lower α -SiAlON phase stability also implies a smaller region for α -SiAlON phase and a larger region for liquid or other competing phases. To synthesize such α -SiAlON crystals, it is prudent to limit the amount of forming liquid addition (see next section) to ensure that the overall composition does yield some α -SiAlON after firing and cooling. This latter consideration dictates that the amount of liquid addition should be less (say, 5–10 wt%) for the less stable Nd- and Mg- α -SiAlON systems than for the more stable Li-, Ca-, Y-, and Yb- α -SiAlON systems (say, 20–40 wt%). When these conditions are not met, α -SiAlON phase becomes unstable and an increasing amount of β -SiAlON phase forms instead according to our experience.

III. Experimental Procedure

Seed crystals of α -SiAlONs with chemical formulas $(\text{Y, Yb, Nd})_{m/3}\text{Si}_{12-m-n}\text{Al}_{m+n}\text{O}_n\text{N}_{16-n}$, $(\text{Ca, Mg})_{m/2}\text{Si}_{12-m-n}\text{Al}_{m+n}\text{O}_n\text{N}_{16-n}$, and $\text{Li}_m\text{Si}_{12-m-n}\text{Al}_{m+n}\text{O}_n\text{N}_{16-n}$ were grown in the liquid phase by heating pelletized powder compacts or loose powders under the conditions shown in Table I. For the purpose of compositional design, the intended α -SiAlON seed composition was selected as $m = 1.5$ and $n = 1.2$, which, if achieved, is likely

R. E. Loehman—contributing editor

Manuscript No. 187201. Received January 16, 2002; approved February 26, 2004. Supported by the U.S. Air Force Office of Scientific Research, under Grant No. F49620-01-1-0150. Facilities at the University of Pennsylvania are supported by the U.S. National Science Foundation under MRSEC Grant No. DMR00-79909.
*Member, American Ceramic Society.

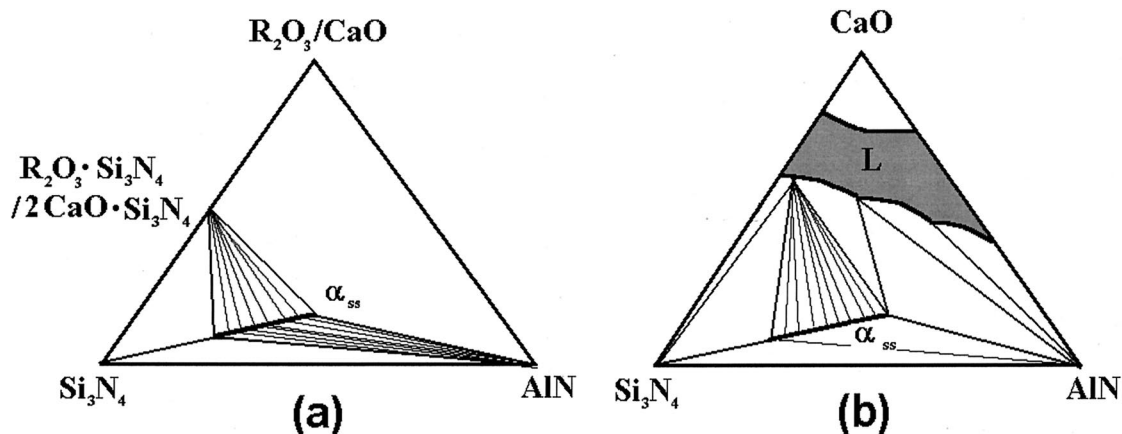


Fig. 1. Schematic (a) subsolidus phase relations in $R_2O_3/CaO-Si_3N_4-AlN$ system and (b) high-temperature phase relations in the $CaO-Si_3N_4-AlN$ system. Adopted from Ref. 34.

to be relatively stable compared with most α -SiAlON compositions.^{16–19} The overall starting composition was then designed to comprise a certain (weight) percentage of the intended α -SiAlON, with the remainder being a forming liquid of a compatible type. The weight percent of the liquid and its intended composition are also listed in Table I.

Starting compositions were prepared from powder mixtures of α - Si_3N_4 (see below), β - Si_3N_4 (SN-F1, Denka Ind., Japan), AlN (type F, Tokuyama Soda Co., CA), Al_2O_3 (AKP50, Sumitomo Chemical America, NY), Y_2O_3 (99.9%, ALFA-Johnson Matthey Co., MA), Yb_2O_3 (99.9%, ALFA-Johnson Matthey Co., MA), Nd_2O_3 (99.9%, ALFA-Johnson Matthey Co., MA), MgO (99+%, Aldrich Chemical Co., WI), $CaCO_3$ (99.9%, CS-3NA, Pred Materials, Inc., NY), and Li_2CO_3 (99+%, Aldrich Chemical Co., WI). Two α - Si_3N_4 powders, one finer (0.5 μm ; SN-E-10, Ube Ind., Japan; shown as “ α ” in Table I) and the other coarser (1.2 μm ; SN-E-03, Ube Ind., Japan; shown as “ α -c” in Table I), were used for comparison. The oxygen content in α - Si_3N_4 (1.24 wt% in SN-E-10 and 0.8% in SN-E-03) and AlN (0.88 wt%) were taken into account in the formulation.

Powder mixtures were attrition milled for 2 h in isopropyl alcohol with high-purity Si_3N_4 milling media, in a Teflon-coated

jar. They were subsequently dried under a halogen lamp while being stirred. To obtain loose powders, dried powder mixtures were sieved through a 125-mesh sieve without further compacting. To obtain pellets, powder mixtures were pressed under 30 MPa of uniaxial pressure at room temperature. To grow crystals, loose powders or compact samples were heated in a boron nitride crucible in a graphite resistance furnace in a nitrogen atmosphere of a controlled pressure (see conditions in Table I).

Fired samples were mechanically crushed, sieved through a 125-mesh sieve, and treated with various chemical solutions to dissolve the residual glass and non-SiAlON phases.^{7,10} Washing in distilled water with ultrasonic stirring then followed each stage of chemical treatment. Qualitative phase analysis of sintered compacts and final seed crystals was conducted by X-ray diffraction using a Rigaku diffractometer with $CuK\alpha$ radiation. Final chemical compositions were estimated (assuming $n = 1.2$ in the α -SiAlON formula) using known empirical relationships between lattice parameters and compositions of Y-, Ca-, and Li- α -SiAlONs.^{17–19} Since it is difficult to separate α -SiAlON from β -SiAlON seed crystals, we will mostly report below those synthesis conditions that yielded α -SiAlON without β -SiAlON.

Table I. Compositions[†] and Processing Conditions

Sample	Composition of forming liquid	Forming liquid [†] (wt%)	Si_3N_4 powder [‡]	T (°C)/time (h)	$P(N_2)$ (MPa)	Initial form
Y-1	0.34 Al_2O_3 :0.31 Y_2O_3 :0.35 Si_3N_4	20	α	1700/2	0.2	Loose
Y-2	0.34 Al_2O_3 :0.31 Y_2O_3 :0.35 Si_3N_4	20	α	1700/2	10	Pellet
Y-3	0.34 Al_2O_3 :0.31 Y_2O_3 :0.35 Si_3N_4	20	α	1900/2	10	Pellet
Y-4	0.34 Al_2O_3 :0.31 Y_2O_3 :0.35 Si_3N_4	20	α	1700/2	10	Loose
Y-5	0.34 Al_2O_3 :0.31 Y_2O_3 :0.35 Si_3N_4	20	α -c	1700/2	0.2	Loose
Y-6	0.34 Al_2O_3 :0.31 Y_2O_3 :0.35 Si_3N_4	40	α	1700/2	0.2	Loose
Y-7	Y_2O_3 : Si_3N_4	20	α	1900/2	10	Pellet
Y-8	Y_2O_3 : Si_3N_4	20	β	1900/2	10	Pellet
Y-9	Y_2O_3 : Si_3N_4	3	α	1900/2	10	Pellet
Ca-1	2 CaO : Al_2O_3 : SiO_2	20	α	1700/2	0.2	Pellet
Ca-2	2 CaO : Al_2O_3 : SiO_2	20	α	1700/2	10	Pellet
Ca-3	0.6 CaO :0.1 AlN :0.3 Si_3N_4	20	α	1700/2	0.2	Pellet
Ca-4	2 CaO : Al_2O_3 : SiO_2	20	α	1900/2	10	Pellet
Ca-5	2 CaO : Al_2O_3 : SiO_2	20	α -c	1700/2	0.2	Pellet
Ca-6	2 CaO : Al_2O_3 : SiO_2	40	α	1700/2	0.2	Pellet
Ca-7	2 CaO : Al_2O_3 : SiO_2	20	α	1700/2 [§]	10	Pellet
Ca-8	2 CaO : Al_2O_3 : SiO_2	20	α	1700/2 [¶]	10	Pellet
Li-1	Li_2O : Al_2O_3 :2 SiO_2	20	α	1700/2	10	Pellet
Li-2	0.45 Li_2O :0.25 AlN :0.3 Si_3N_4	20	α	1900/2	10	Pellet
Mg-1	0.6 MgO :0.15 AlN :0.25 Si_3N_4	5	α	1900/2	10	Pellet
Nd-1	Nd_2O_3 : Si_3N_4	10	α	1850/2	10	Loose
Yb-1	0.13 Al_2O_3 :0.52 Yb_2O_3 :0.35 Si_3N_4	20	α	1650/2	10	Loose

[†]Overall composition obtained by adding the percentage (in the third column) of a forming liquid (of the composition in the second column) and the balance percentage of the intended α -SiAlON, which all has $m = 1.5$ and $n = 1.2$. [‡]c for coarse powders. See text. [§]Heated at 1°C/min. [¶]Heated at 30°C/min.

The size and morphology of seed crystals were studied by scanning electron microscopy (SEM) (JEOL-6300F). Statistics were collected from 150 to 200 crystals revealed by SEM images. In general, the data reported below refer to the harvested seed crystals, which were a subset (about 70%¹⁰) of the entire α -SiAlON crystal populations in the fired samples. Although the statistics of the subset may differ from those of the entire population, very likely it still reflects the same overall trend in crystal size and morphology of the latter. Therefore, it will be used to identify the key factors that influence the kinetics of seed synthesis in these complicated systems.

IV. Results

A range of experimental variables including compositions, powder mixtures, and firing conditions (temperature, nitrogen pressure, and heating rate) were studied to identify the key factors that influence the final size and morphology of seed crystals. Table II summarizes the phase assemblage, size, and aspect ratio (length/width) of the final seeds along with their statistical distributions. According to these observations the primary effects of composition and processing conditions are described below.

(1) Temperature

A dramatic increase in crystal size was seen with increasing temperature. Figures 2(a,b) show the SEM images of Ca-2 and Ca-4 prepared at 1700° and 1900°C, respectively. Seeds grown at 1900°C were much larger. The same effect can be seen for other compositions (Y-2 and Y3; Li-1 and Li-2). This general trend suggests that liquid viscosity, which decreases with increasing temperature, may be of primary importance. We also found that the faster growth was often accompanied by a decrease in aspect ratio. Such a trend is similar to the one seen in late-stage anisotropic Ostwald ripening; for example, Kitayama *et al.*²⁰ observed the same trend for β -Si₃N₄ seeds, prepared at 1750°–1900°C.

(2) Amount of Liquid Addition in the Composition

The actual amount of the liquid during crystal growth is difficult to estimate. This is because of the transient nature of phase

transformation in the silicon nitride system, which involves dissolution of the starting powders and reprecipitation of equilibrium crystals. Nevertheless, it is certain that the compositions that are comprised of a larger percentage of the forming liquid addition must have more liquid at all stages of reactions. Comparing compositions of different liquid percentages in Table I, we found an increased amount of liquid did not always result in an increased width of the grown crystals; rather, it led to a higher aspect ratio. Figures 3(a,b) show the microstructures of Y-7 and Y-9 seeds grown at 1900°C with 20% and 3% liquid, respectively. Less liquid resulted in less elongated seed crystals. A similar observation at 1700°C was already reported earlier.¹⁰ The same trend can be seen for other compositions (Y-1 and Y-6; Ca-1 and Ca-6). However, the width of the crystals was not sensitive to the amount of the liquid used. This suggests that the influence of the amount of liquid on aspect ratio could be due to the postponement of crystal impingement. Also, the addition of the liquid, which is relatively rich in oxygen, dilutes the nitrogen content in the overall composition, thus lowering viscosity and promoting growth.

(3) Nitrogen Pressure

Figures 4(a,b) show the microstructures of samples (Y-1 and Y-4, initially as loose powders) fired at 1700°C under 0.2 and 10 MPa of nitrogen pressure, respectively. Also shown are the seed crystals recovered from these samples. It is clear that sintering had occurred, resulting in relatively dense regions. (Open porosity was still present in these samples, however.) The size of the dense regions was larger at higher pressure (Fig. 4(b)), indicating a pressure effect on aiding sintering. Meanwhile, larger and highly elongated crystals were found under a higher pressure, indicating a pressure effect on promoting crystal growth.

(4) Green Density

To determine whether the size of the dense regions is critical for seed morphology or not, we compare the microstructures in Figs. 4(a,b) with that in Fig. 4(c). These micrographs were all taken from samples of the same composition and fired at the same temperature, except Fig. 4(c) was not made from loose powder but from a pellet (Y-2). (It was sintered under 10 MPa of nitrogen

Table II. Phase Identification and Microstructure of Seeds[†]

Sample	Phase assemblage [‡] after firing and cooling	a/c (Å/Å)		W (μm)	AR	AR-5%
		Lattice parameters [§]	Reference lattice parameter [¶]			
Y-1	Glass, M, 12H	7.828(2)/5.705(2)	7.826(2)/5.707(2)	0.42 ± 0.10	2.2 ± 1.2	5.6
Y-2	Glass, M, 12H	7.824(3)/5.703(2)		0.49 ± 0.13	2.0 ± 1.1	4.9
Y-3	Glass, M, 12H, β'	7.834(3)/5.707(3)		1.68 ± 0.97	2.7 ± 1.4	5.4
Y-4	Glass, 12H	7.832(2)/5.706(1)		0.71 ± 0.19	2.4 ± 1.3	6.3
Y-5	Glass, M, 12H	7.826(2)/5.704(2)		0.45 ± 0.10	2.3 ± 1.2	5.8
Y-6	Glass, M, 12H	7.836(1)/5.710(2)		0.40 ± 0.12	2.9 ± 1.3	6.0
Y-7	Glass, M	7.840(3)/5.713(1)		3.51 ± 2.64	3.1 ± 1.7	6.9
Y-8	Glass, M	7.837(2)/5.711(3)		1.34 ± 0.96	3.5 ± 1.9	6.1
Y-9	M	7.827(3)/5.704(1)		4.45 ± 1.97	1.4 ± 0.4	2.3
Ca-1	Glass	7.837(1)/5.701(1)	7.840(1)/5.704(2)	0.33 ± 0.10	2.6 ± 1.6	5.8
Ca-2	Glass	7.843(1)/5.707(1)		0.45 ± 0.11	3.8 ± 2.2	8.2
Ca-3	Glass	7.853(2)/5.714(2)		0.33 ± 0.08	3.3 ± 1.8	7.7
Ca-4	Glass	7.841(1)/5.704(1)		1.61 ± 0.75	2.7 ± 1.8	5.4
Ca-5	Glass	7.850(2)/5.702(3)		0.42 ± 0.11	3.0 ± 1.8	7.3
Ca-6	Glass	7.859(2)/5.711(2)		0.43 ± 0.11	4.3 ± 2.8	10.1
Ca-7	Glass	7.848(2)/5.709(1)		0.30 ± 0.11	2.2 ± 1.8	5.1
Ca-8	Glass	7.837(2)/5.710(2)		0.38 ± 0.13	3.7 ± 2.0	7.8
Li-1	Glass, Li-eucryptite	7.817(2)/7.679(2)	7.822(1)/5.673(2)	0.28 ± 0.08	1.6 ± 0.5	2.5
Li-2	Glass, 12H	7.819(2)/7.681(3)		2.12 ± 1.28	1.1 ± 0.3	1.6
Mg-1	Glass, Mg-polytype ^{††}	7.798(2)/5.663(2)	7.803(3)/5.662(2)	2.75 ± 1.63	1.2 ± 0.3	1.5
Nd-1	Glass, M, 12H, β	7.846(2)/5.713(1)	7.833(2)/5.710(2)	0.92 ± 0.51	4.3 ± 1.9	8.4
Yb-1	Glass, M	7.821(2)/5.702(3)	7.824(2)/5.704(2)	0.61 ± 0.16	2.1 ± 1.2	5.6

[†]W for crystal width, AR for average aspect ratio, AR-5% for the highest 5% aspect ratio. [‡]Other than α -SiAlON, which was present in all samples. M for melilite, β' for β -SiAlON. [§]For α -SiAlON. [¶]For α -SiAlON with $m = 1.5$ and $n = 1.2$. ^{††}JCPDS Card No. 48-1605 (Mg_{3,29}Si_{1,89}Al_{2,82}O_{4,41}N_{4,59}).

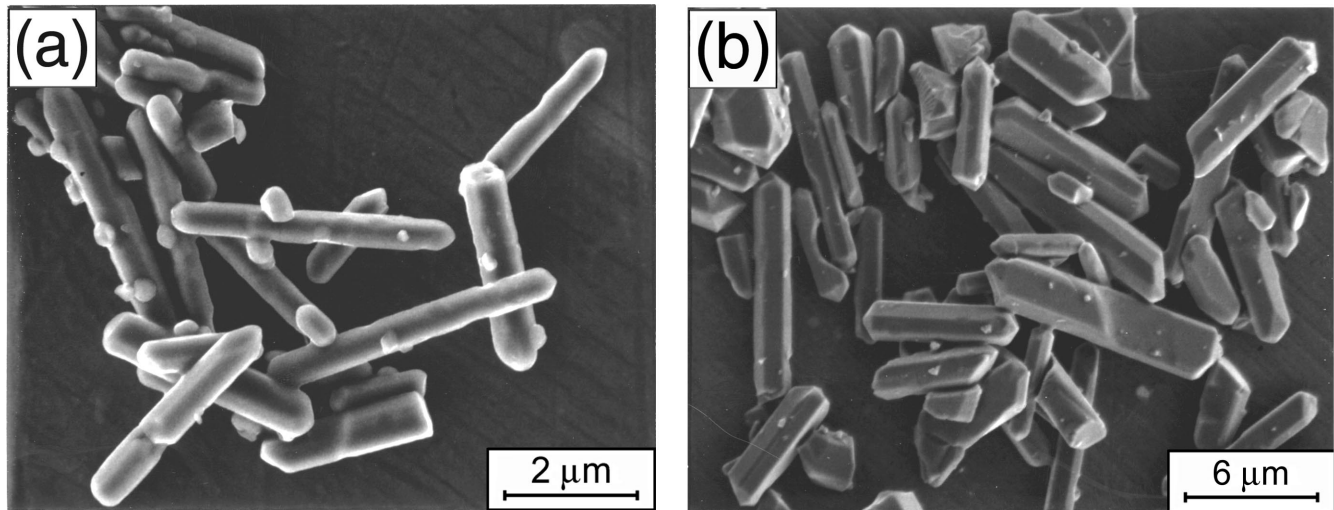


Fig. 2. SEM micrographs of Ca- α -SiAlON seeds grown at (a) 1700° and (b) 1900°C. They correspond to Ca-2 and Ca-4 in the Tables.

pressure, the same pressure used for Fig. 4(b).) Because of the higher green density in this sample, the fired density was much higher and the porosity much lower. Very large dense regions were evident throughout the sample. Yet the average crystal size of Y-2 (see both Fig. 4(c) and Table II) was smaller than that of Y-4 (Fig. 4(b)), which was fired from loose powders under the same condition. Indeed, the crystal size of Y-2 was close to that of Y-1 (Fig. 4(a)) that was also from loose powders but fired at a lower nitrogen pressure. This demonstrates that a higher green density, which results in a larger size of the dense regions, actually leads to a smaller crystal size. They also imply that the nitrogen pressure effect of promoting crystal growth is intrinsic and not due to the density increase noted in (c).

(5) Starting Silicon Nitride Powders

It is well known that the phase content and particle size of silicon nitride powders have a direct effect on the microstructure of silicon nitride and SiAlON ceramics.^{1,21-23} To investigate the size effect, samples (Y-1 and Y-5; also Ca-1 and Ca-5) of identical composition were prepared using α -Si₃N₄ powders with two average particle sizes, 0.5 μ m (SN-E10) and 1.2 μ m (SN-E3), respectively. The final crystal size and aspect ratio were found to be slightly larger when coarser α powders were used. Assuming preferential nucleation of α -SiAlON on α -Si₃N₄, coarser α powders should result in fewer α -SiAlON nuclei, which should grow

to larger sizes and more elongated shapes because of less competition and impingement. On the other hand, since the starting powders must progressively dissolve to provide the source materials for newly precipitated crystals, it is necessary to consider the driving force for dissolution, which is smaller for coarser starting powders than for finer ones. This would in turn result in a smaller driving force for crystal growth, negating the nucleation advantage of coarser powders. Apparently, the competition between these two effects rendered the benefit of using coarse α powders in promoting growth relatively insignificant.

The competing effects of nucleation and growth kinetics were also seen in the experiments comparing α/β -Si₃N₄ powders. Figures 5(a,b) show the SEM micrographs of Y-7 and Y-8 samples, prepared from α - and β -Si₃N₄, respectively. Many larger, elongated grains were observed in the former case, Fig. 5(a). If nucleation consideration is of primary importance, then we would expect more nuclei present in the α -Si₃N₄ route, which leads to more numerous but smaller crystals. On the other hand, since the driving force for α -Si₃N₄ dissolution is larger than that for β -Si₃N₄, due to the better phase stability of the latter, the α -Si₃N₄ route should result in faster kinetics if the driving force consideration is of primary importance.^{21,22} Our experimental observations in Fig. 5 indicated that the effect of driving force dominated over the nucleation consideration.

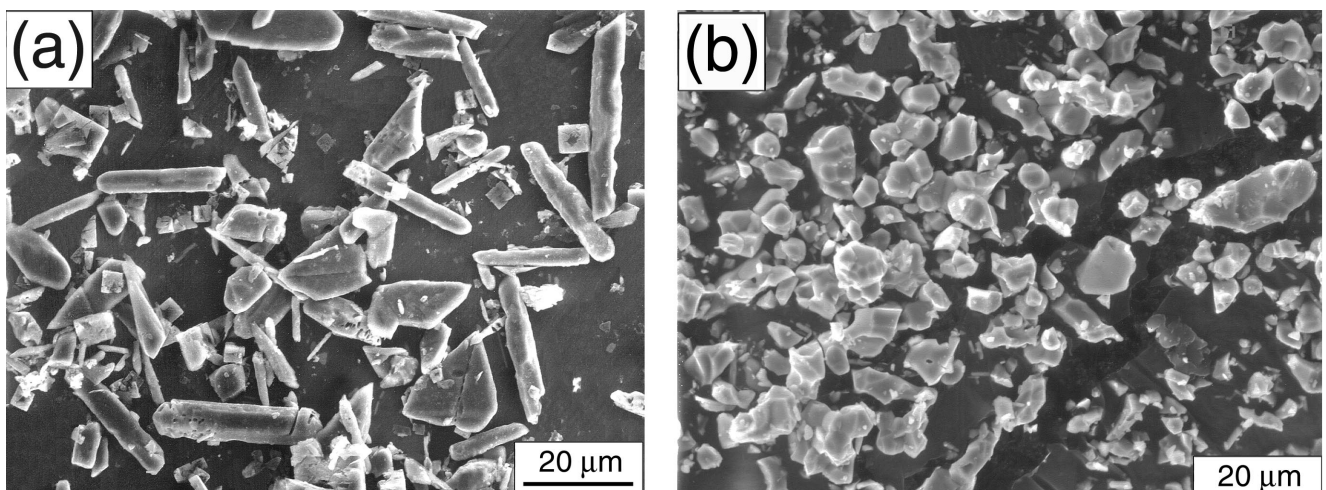


Fig. 3. SEM micrographs of Y- α -SiAlON seeds grown at 1900°C in (a) 20% and (b) 3% of liquid. They correspond to Y-7 and Y-9 in the Tables.

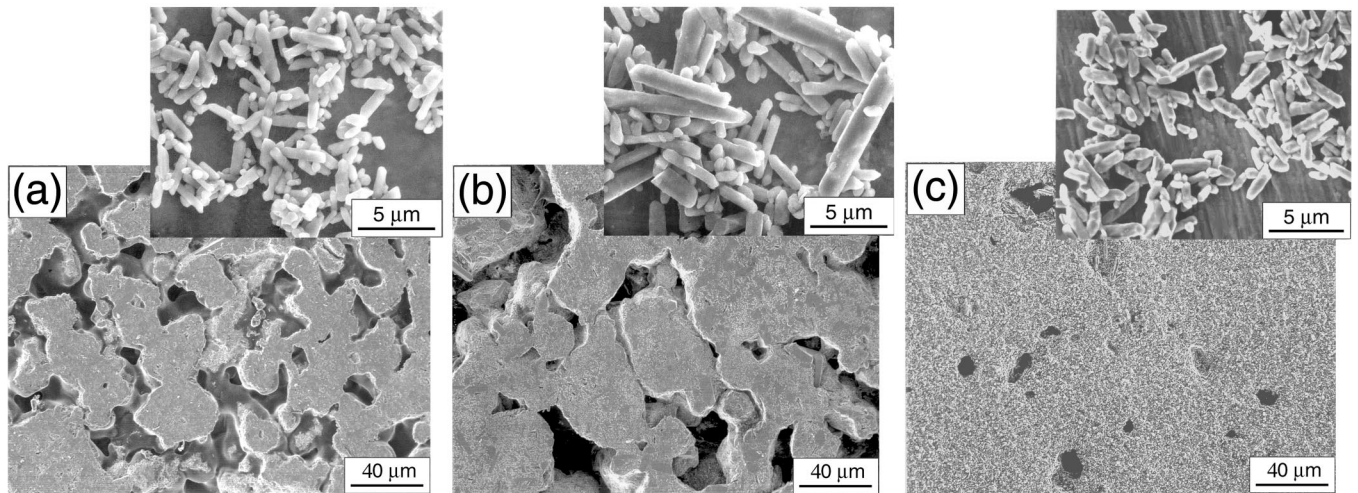


Fig. 4. SEM micrographs of seeds grown at 1700°C under various nitrogen pressures and starting forms: (a) 0.2 MPa, initially loose powders; (b) 10 MPa, initially loose powders; and (c) 10 MPa, initially pellet. They correspond to Y-1, Y-4, and Y-2 in the Tables.

(6) Heating Rates

Heating schedule, such as two-step sintering and heating rate, has been shown to play an important role in the microstructure control of α -SiAlON ceramics.^{1,8,24,25} To investigate this aspect, powder mixtures of Ca-7 and Ca-8 were heated to 1700°C with heating rates of 1 and 30°C/min, respectively. Both the crystal size and the aspect ratio were found to increase with the heating rate. Previously, we found a slower heating rate to cause more α -SiAlON nuclei to form at low temperatures, which then compete with each other for growth at high temperatures, giving rise to smaller and less elongated crystals.²⁵ A slower heating rate also allows more reaction (from starting powders to α -SiAlON) to proceed at lower temperatures, leaving less liquid to higher temperature reactions that promote rapid growth. This too can lead to smaller crystals. The two effects are parallel and both are consistent with our results.

(7) Effect of Modifying Elements

Morphologies of SiAlON crystals stabilized by different cations (Mg, Li, Yb, Y, Nd, Ca) are compared in Fig. 6. Here the comparison can be made using either the average aspect ratio or the maximum aspect ratio, both yielding similar trends. In Fig. 6, the mean aspect ratios of seeds in the highest 5% of the statistical distributions are plotted as an example. These data involve various

growth conditions, which, for clarity, are roughly indicated in two sets: low-temperature growth (1650°–1700°C, open circles) and high-temperature growth (1850°–1900°C, filled circles.) Despite different growth conditions, a positive correlation between the aspect ratio and the ionic radius is evident. Hoffmann *et al.*²⁶ observed a similar effect of rare-earth cations on the aspect ratio of β -Si₃N₄ crystals, grown in (Si,Al,M)(O,N) liquids at low volume fractions (about 5–10 vol% of crystals). They attributed such effect to the cation segregation to the crystal/liquid interface. In view of the similar crystallographic nature of α -SiAlON and β -Si₃N₄, it is likely that these two observations share the same origin.

V. Discussion

Our phase analysis is summarized in Table II. It confirms that α -SiAlON is formed, whereas β -SiAlON and α/β -Si₃N₄ were absent. Therefore, the compositions chosen were largely in the compatibility region bordered by α -SiAlON, liquid, and in some cases other competing phases, which become stable either at the firing temperature or during cooling. The reactions were most likely complete, i.e., equilibrium was achieved, given the relatively large amount of forming liquid present in our compositions. In the literature of β -Si₃N₄ seed crystals, Ramesh *et al.*² found that even an addition of 0.5 wt% of Y₂O₃ to α -Si₃N₄ was sufficient to

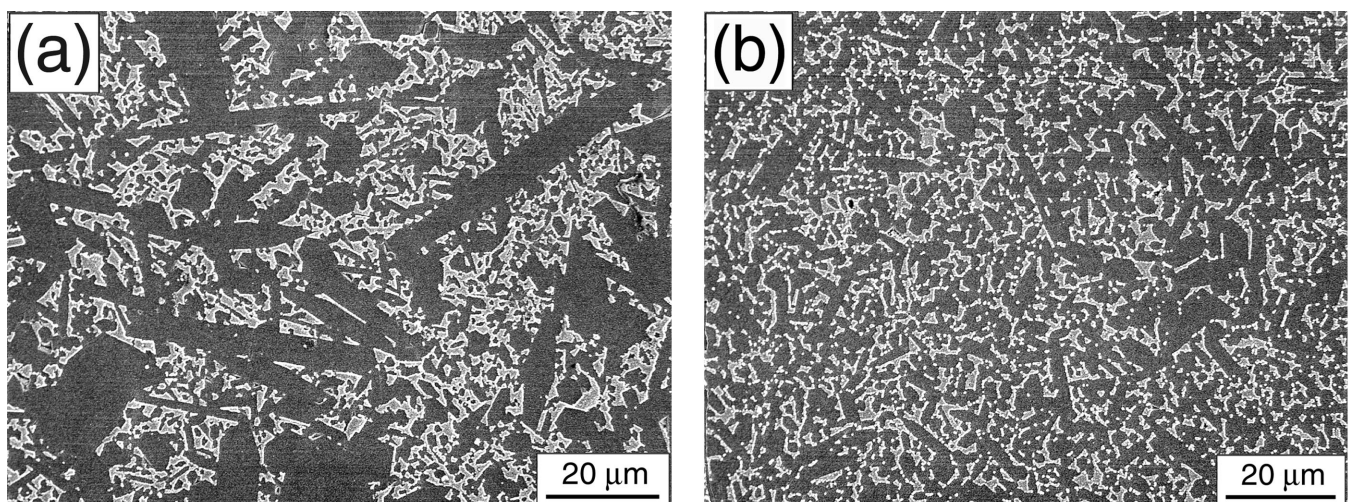


Fig. 5. SEM micrographs of Y- α -SiAlON seeds prepared from (a) α -Si₃N₄ and (b) β -Si₃N₄ starting powders. They correspond to Y-7 and Y-8 in the Tables.

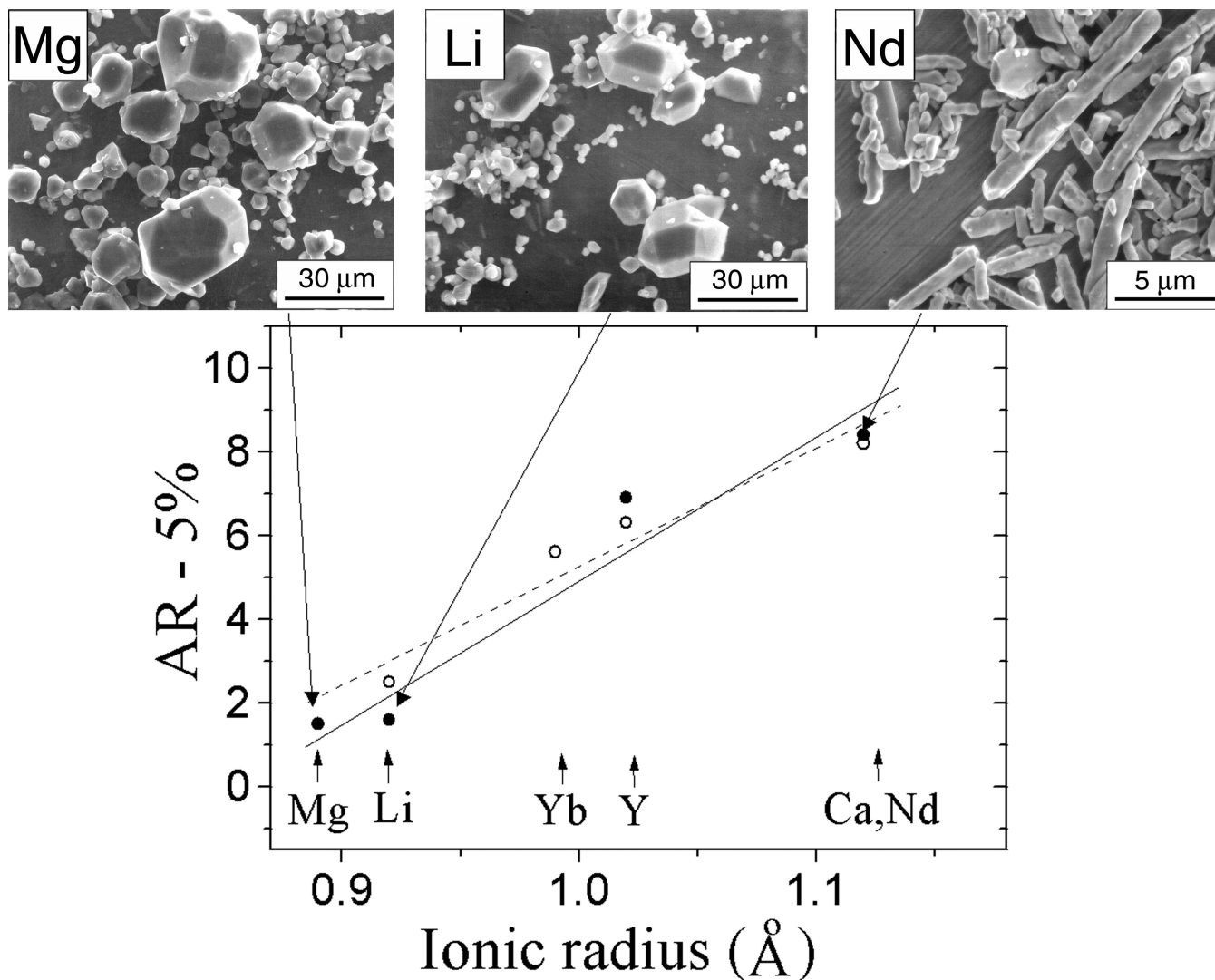


Fig. 6. Mean aspect ratio as function of the ionic radius of modifying cation in α -SiAlON. Also shown are SEM micrographs of Mg-, Li-, and Nd- α -SiAlON crystals. Firing temperatures are 1850–1900°C (filled symbols) and 1650–1700°C (open symbols).

completely transform the starting powders into elongated β - Si_3N_4 crystals. Our observations on full α - $\text{Si}_3\text{N}_4 \rightarrow \alpha$ -SiAlON transformation even at low liquid content are in agreement with their results. Ramesh *et al.*² also found their crystals to possess an average aspect ratio of 3–4. Our study, however, found that the aspect ratio of α -SiAlON crystals grown with a small amount of liquid was much smaller, 1.4 for Y-9 and 1.2 for Mg-1. Therefore, there are some essential differences between the crystal growth of α -SiAlON and of β - Si_3N_4 , even though the basic mechanism of liquid-assisted crystal growth must be similar in both cases.

The robust growth of β - Si_3N_4 despite the small amount of liquid may be attributed to the large driving force of $\alpha \rightarrow \beta$ transformation and the nucleation statistics of β - Si_3N_4 crystals. In Remesh *et al.*'s experiment,² the fraction of β -nuclei was 4% while the remaining 96% of starting powders were α - Si_3N_4 , which dissolved and reprecipitated on those β - Si_3N_4 nuclei. It is known that large aspect ratios can rapidly develop during $\alpha \rightarrow \beta$ transformation.^{27–29} On the other hand, all 96% of the starting α - Si_3N_4 powder was capable of nucleating α -SiAlON crystals.^{1,30} Therefore, the transformation to the α -SiAlON phase was rapidly completed and the α - $\text{Si}_3\text{N}_4 \rightarrow \alpha$ -SiAlON driving force was exhausted. Subsequent growth must then take place by Ostwald ripening, which has a much smaller driving force, as it is due to capillarity rather than phase transformation. In the latter case much liquid is required to facilitate the formation of elongated grains. This makes the formation of large needlelike grains easier by

postponing impingement between α -SiAlON crystals, and lowering viscosity and kinetic barrier (see Section IV(2)). The importance of the driving force was also seen in our comparison of α and β starting powders. Smaller and less elongated α -SiAlON crystals were grown using β powders (see Fig. 5), which have a lower driving force for dissolution than α powders.

In the experiments of Ramesh *et al.*² that used 0.5 wt% of Y_2O_3 as additive, the amount of the liquid during reactions was obviously too small to form large dense regions and completely wet all the silicon nitride particles. Indeed, below 1800°C they observed a large amount of untransformed α - Si_3N_4 that was probably associated with unwetted particles. Nevertheless, the β - Si_3N_4 crystals derived from the β -nuclei can grow with the aid of a small amount of wetting liquid. We believe this growth proceeds by a mechanism similar to the so-called vapor–liquid–solid (VLS) mechanism for whisker growth.³¹ In this mechanism an isolated crystal grows from a layer of liquid, which is supplied with the source material by vapor condensation in VLS, or by α - Si_3N_4 dissolution in Ramesh *et al.*'s experiment.² No impingement is encountered since the powder packing is loose and there is plenty of open space for crystals to grow into. Therefore, the aspect ratio of anisotropic growth is limited only by the amount of α - Si_3N_4 available.

In contrast, in the synthesis of α -SiAlON crystals, a larger amount of transient liquid forms (due to interstitial cations in α -SiAlON structure), which leads to the formation of dense regions of various sizes after certain firing time. In the pelletized

samples, relatively large dense regions are formed in the first stage of liquid-phase sintering, when the liquid content is high and very rapid densification is experienced.^{32,33} Since the number density of α -SiAlON crystals in the dense regions is also high, such crystals must encounter impingement from the very beginning. Therefore, they have little chance for constraint-free growth, which is required for developing a high aspect ratio. This explains why only crystals with small aspect ratios are observed in Fig. 4(c), which shows a pelletized sample. Even in the loose powders, patches of dense regions eventually form. Such regions exert a constraint on crystal growth if the crystals are considerably smaller than the dimensions of dense regions, i.e., if the crystal does not have an access to the “free” boundary of the dense region. In our experiments, the length of a large crystal is of the order of several micrometers. So we expect dense regions of several tens of micrometers in size should exert the constraint. A closer look at Fig. 4 confirms that the typical size of dense regions is an order of magnitude larger than the crystal size. Therefore, growing crystals shown in Fig. 4 must experience strong effects of impingement. This situation is partly alleviated for regions that contain more liquid, which is also consistent with our observations (see Section IV(2)).

Lastly, the nitrogen pressure effect can be understood by its role in suppressing nitrogen loss and maintaining a relatively high supersaturation, thus promoting crystal growth. Such effect is likely to be significant in the early stage of firing, when the dense regions are still too small to exert a constraint on crystal growth. Pressure, meanwhile, can also assist sintering by providing an additional driving force to remove internal pores. This effect becomes important at a later stage when larger, pore-closing aggregates have formed. However, since crystal growth in such large aggregates is most likely already constrained, the pressure effect on forming larger dense regions does not directly affect the development of aspect ratio. The micrographs of Figs. 4(a,b), which show that larger and more highly elongated crystals were found under a higher pressure, are consistent with this interpretation.

VI. Conclusions

(1) Seed crystals of α -SiAlON of various size and morphology have been obtained for several systems. Elongated seeds are readily obtained for Yb-, Y-, Nd-, and Ca- α -SiAlONs using the synthesis conditions provided by this study.

(2) Systematic effects of firing temperature, amount of liquid addition, nitrogen pressure, green density, starting powders, and heating rate on the size and morphology of seed crystals have been investigated. These effects can be understood based on the kinetics of α -SiAlON formation and the microstructure development during liquid-phase sintering.

(3) Major differences between seed crystal formation of β -Si₃N₄ and α -SiAlON have been identified. They reflect the fact that α -SiAlON formation enjoys plentiful nucleation sites, and that the growth mostly occurs in the stage of Oswald ripening. Especially important is the sensitivity of aspect ratio to liquid amount, which lessens the impingement effect. The latter factor is apparently less crucial for growing β -Si₃N₄ seeds.

(4) A positive correlation between the aspect ratio of seed crystals and the ionic radii of the modifying cations in α -SiAlON has been found. Such a relation mirrors a similar one previously known for β -Si₃N₄ and β -SiAlON.

References

¹I-W. Chen and A. Rosenflanz, “A Tough SiAlON Ceramic Based on α -Si₃N₄ with a Whisker-like Microstructure,” *Nature (London)*, **389**, 701–704 (1997).
²P. D. Ramesh, R. Oberracker, and M. J. Hoffmann, “Preparation of β -Silicon Nitride Seeds for Self-Reinforced Silicon Nitride Ceramics,” *J. Am. Ceram. Soc.*, **82** [6] 1608–10 (1999).

³S. Y. Lee, K. A. Appagyeyi, and H. D. Kim, “Effect of β -Si₃N₄ Seed Crystal on the Microstructure and Mechanical Properties of Sintered Reaction Bonded Silicon Nitride,” *J. Mater. Res.*, **14** [1] 178–84 (1999).
⁴K. Hirao, T. Nagaoka, M. E. Brito, and S. Kanzaki, “Microstructure Control of Silicon Nitride by Seeding with Rodlike β -Silicon Nitride Particles,” *J. Am. Ceram. Soc.*, **77** [7] 1857–62 (1994).
⁵P. F. Becher, E. Y. Sun, K. P. Plucknett, K. B. Alexander, C. H. Hsueh, H. T. Lin, S. B. Waters, C. G. Westmoreland, E. S. Kang, K. Hirao, and M. E. Brito, “Microstructural Design of Silicon Nitride with Improved Fracture Toughness: I, Effects of Grain Shape and Size,” *J. Am. Ceram. Soc.*, **81** [11] 2821–30 (1998).
⁶H. Imamura, K. Hirao, M. E. Brito, M. Toriyama, and S. Kanzaki, “Further Improvement in Mechanical Properties of Highly Anisotropic Silicon Nitride Ceramics,” *J. Am. Ceram. Soc.*, **83** [3] 495–500 (2000).
⁷K. Hirao, A. Tsuge, M. E. Brito, and S. Kanzaki, “Preparation of Rod-like β -Si₃N₄ Single Crystal Particles,” *J. Ceram. Soc. Jpn.*, **101** [9] 1078–80 (1993).
⁸J. Kim, A. Rosenflanz, and I-W. Chen, “Microstructure Control of *In Situ* Toughened α -SiAlON Ceramics,” *J. Am. Ceram. Soc.*, **83** [7] 1819–21 (2000).
⁹W. W. Chen, W. Y. Sun, Y. W. Li, and D. S. Yan, “Microstructure of (Y+Sm)- α -SiAlON with α -SiAlON Seeds,” *J. Mater. Res.*, **15** [10] 2223–27 (2000).
¹⁰M. Zenotchkine, R. Shuba, J.-S. Kim, and I-W. Chen, “Synthesis of α -SiAlON Seed Crystals,” *J. Am. Ceram. Soc.*, **84** [7] 1651–53 (2001).
¹¹(a) M. Zenotchkine, R. Shuba, J.-S. Kim, and I-W. Chen, “R-Curve Behavior of *In Situ* Toughened α -SiAlON Ceramics,” *J. Am. Ceram. Soc.*, **84** [4] 884–26 (2001). (b) M. Zenotchkine, R. Shuba, J.-S. Kim, and I-W. Chen, “Effect of Seeding on the Microstructure and Mechanical Properties of α -SiAlON: I, Y-SiAlON,” *J. Am. Ceram. Soc.*, **85** [5] 1254–59 (2002). (c) R. Shuba and I-W. Chen, “Effect of Seeding on the Microstructure and Mechanical Properties of α -SiAlON: II, Ca-SiAlON,” *J. Am. Ceram. Soc.*, **85** [5] 1260–67 (2002). (d) M. Zenotchkine, R. Shuba, and I-W. Chen, “Effect of Seeding on the Microstructure and Mechanical Properties of α -SiAlON: III, Comparison of Modifying Cations,” *J. Am. Ceram. Soc.*, **86** [7] 1168–75 (2003).
¹²C. L. Hewett, Y. B. Cheng, B. C. Muddle, M. B. Trigg, “Thermal Stability of Calcium α -Sialon Ceramics,” *J. Eur. Ceram. Soc.*, **18** [4] 417–27 (1998).
¹³Z.-K. Huang and I-W. Chen, “Rare-Earth Melilite Solid Solution and Its Phase Relations with Neighboring Phases,” *J. Am. Ceram. Soc.*, **79** [8] 2091–97 (1996).
¹⁴Z.-K. Huang and D.-S. Yan, “Phase Relationships in Si₃N₄-AlN-M₂O₃ System and Their Implications for Sialon Fabrication,” *J. Mater. Sci.*, **27**, 5640–44 (1992).
¹⁵K. H. Jack, “SiAlONs and Related Nitrogen Ceramics,” *J. Mater. Sci.*, **11**, 1135–58 (1976).
¹⁶A. Rosenflanz and I-W. Chen, “Phase Relationships and Stability of α -SiAlON,” *J. Am. Ceram. Soc.*, **82** [4] 1025–36 (1999).
¹⁷W.-Y. Sun, T.-Y. Tien, and T.-S. Yen, “Solubility Limits of α -SiAlON Solid Solutions in the System Si₃N₄-Y₂O₃,” *J. Am. Ceram. Soc.*, **74** [10] 2547–50 (1991).
¹⁸J. W. T. van Rutten, H. T. Hitzner, and R. Metselaar, “Phase Formation of Ca α -SiAlON by Reaction Sintering,” *J. Eur. Ceram. Soc.*, **16**, 995–99 (1996).
¹⁹Z. B. Yu, D. P. Thompson, and A. R. Bhatti, “Preparation of Single Phase Lithium α -Sialon,” *Br. Ceram. Trans.*, **97** [2] 41–47 (1998).
²⁰M. Kitayama, K. Hirao, M. Toriyama, and S. Kanzaki, “Control of β -Si₃N₄ Crystal Morphology and Its Mechanism. Part 1. Effect of SiO₂ and Y₂O₃,” *J. Ceram. Soc. Jpn.*, **107** [10] 930–34 (1999).
²¹A. Rosenflanz and I-W. Chen, “Kinetics of Phase Transformations in SiAlON Ceramics: I. Effects of Cation Size, Composition and Temperature,” *J. Eur. Ceram. Soc.*, **19**, 2325–35 (1999).
²²A. Rosenflanz and I-W. Chen, “Kinetics of Phase Transformations in SiAlON Ceramics: II. Reaction Paths,” *J. Eur. Ceram. Soc.*, **19**, 2337–48 (1999).
²³M. J. Hoffmann and G. Petzow, “Microstructural Design of Si₃N₄ Based Ceramics,” *Mater. Res. Soc. Symp. Proc.*, **287**, 3–14 (1993).
²⁴C. Zhang, E. Narimatsu, K. Komeya, J. Tatami, and T. Meguro, “Control of Grain Morphology in Ca- α -Sialon by Changing the Heating Rate,” *J. Mater. Lett.*, **43**, 315–19 (2000).
²⁵M. Zenotchkine, R. Shuba, and I-W. Chen, “Effect of Heating Schedule on the Microstructure and Fracture Toughness of α -SiAlON: Cause and Solution,” *J. Am. Ceram. Soc.*, **85** [7] 1882–84 (2002).
²⁶M. J. Hoffmann, H. Gu, and R. M. Cannon, “Influence of the Interfacial Properties on Microstructural Development and Properties of Si₃N₄ Ceramics,” *Mater. Res. Soc. Symp. Proc.*, **586**, 65–74 (2000).
²⁷N. Kramer, M. J. Hoffmann, and G. Petzow, “Grain Growth Kinetics of Si₃N₄ during α/β Transformation,” *Acta Metall. Mater.*, **41** [10] 2939–47 (1993).
²⁸L. Wang, T.-Y. Tien, and I-W. Chen, “Formation of β -Silicon Nitride Crystals from (Si,Al,Mg,Y)(O,N) Liquid: I, Phase, Composition and Shape Evolutions,” *J. Am. Ceram. Soc.*, **86** [9] 1578–85 (2003).
²⁹L. Wang, T.-Y. Tien, and I-W. Chen, “Formation of β -Silicon Nitride Crystals from (Si,Al,Mg,Y)(O,N) Liquid: II, Population Dynamics and Coarsening Kinetics,” *J. Am. Ceram. Soc.*, **86** [9] 1586–91 (2003).
³⁰S.-L. Huang and I-W. Chen, “Nucleation and Growth of α -SiAlON on α -Si₃N₄,” *J. Am. Ceram. Soc.*, **77** [7] 1711–18 (1994).
³¹R. S. Wagner and W. C. Ellis, *Appl. Phys. Lett.*, **4**, 89 (1964).
³²S.-L. Hwang and I-W. Chen, “Reactive Hot-Pressing of α' - and β' -SiAlON Ceramics,” *J. Am. Ceram. Soc.*, **77** [1] 165–71 (1994).
³³M. Menon and I-W. Chen, “Reaction Densification of α' -SiAlON: II, Densification Behavior,” *J. Am. Ceram. Soc.*, **78** [3] 553–59 (1995).
³⁴A. E. McHale (Ed.), *Phase Equilibria Diagrams—Phase Diagrams for Ceramists*, Vol. 10, *Borides, Carbides, and Nitrides*. American Ceramic Society, Westerville, OH, 1994. □